Supporting information

Zeolitic Imidazolate Framework/Prussian Blue Analogue derived $CoSe_2/FeSe_2$ Heterostructure for Long-Cycle Aluminum-ion Battery

Tianming Liu [a], Meng Liu [b], Juchen Guo [c], Changchun Zhao [a, *], Hao Liu [a], Xiaowei Li [b], Libing Liao [b], Guocheng Lv [b, *]

[a] School of Science, China University of Geosciences, Beijing, 100083, China.

E-mail: zhaocc@cugb.edu.cn

[b] Engineering Research Center of Ministry of Education for Geological Carbon Storage and Low Carbon Utilization of Resources, Beijing Key Laboratory of Materials Utilization of Nonmetallic Minerals and Solid Wastes, National Laboratory of Mineral Materials, School of Materials Science and Technology, China University of Geosciences (Beijing), 100083, China.

E-mail: guochenglv@cugb.edu.cn

[c] Department of Chemical and Environmental Engineering, University of California, Riverside, California 92521, United States; Materials Science and Engineering Program, University of California, Riverside, California 92521, United States.

E-mail: jguo@engr.ucr.edu

Experimental Section

Synthesis of ZIF-67 nanocubes: The ZIF-67 nanocube was prepared by a typical surfactant control method. First, 0.29g $Co(NO_3)_2 \cdot 6H_2O$ and 5 mg cetrimonium bromide (CTAB) were added to 10 mL of deionized water and stirred for 10 min. The solution was added to 70 mL aqueous solution containing 4.54 g of 2-methylimidazole (2-MeIM) and stirred at room temperature for 30 min. After standing for 24 h, centrifuge three times each with water and alcohol, and dry overnight at 60°C.

Synthesis of ZIF-67/Co-Fe PBA core-shell nanocubes: 50 mg of ZIF-67 was dispersed in 30 ml ethanol by ultrasound for at least 10 min. Then 100 mg of $K_3[Fe(CN)_6]$ dissolved in 10 ml of deionized water was added to the above solution and stirred for 2 hours. Finally, the products were collected by centrifugation and washed with water and ethanol for several times, and dry overnight at 60°C.

Synthesis of $CoSe_2/FeSe_2$ hollow nanocubes: The prepared ZIF-67/Co-Fe PBA and Se powders were mixed evenly at a mass ratio of 1:2, and then heated to 300 °C for 4 hours with a heating rate of 2 °C/min under argon atmosphere. After cooling to room temperature, $CoSe_2/FeSe_2$ heterostructure was obtained. Similarly, the precursor of ZIF-67 was mixed with selenium at a mass ratio of 1:2 and heated to 600 °C for 2 hours to get $CoSe_2$.

Characterization

The crystal structure is characterized by X-ray diffraction (XRD; Bruker D8 focus Advance diffractometer with Cu Kα radiation (λ = 1.5406 Å), 40 kV/40 mA). The surface chemical analysis was performed with an X-ray photoelectron spectrometer (XPS; Thermo Fischer, ESCALAB 250XI). All XPS spectra are corrected with C 1s at 284.80 eV. The morphology and structure of the materials were examined by a field emission scanning electron microscope (FESEM; SU-8010) and a transmission electron microscope (TEM; JEM). The Quantachrome Autosorb-iQ volumetric system was used for Brunauer-Emmett-Teller (BET) surface area and pore size analysis. Thermogravimetric analysis (TGA) was performed under airflow at 10 °C min^{-1} using a TA Discovery thermal analyzer.

Electrochemical Measurements

The electrochemical tests were conducted utilizing Swage lok cells (with an internal diameter of 12 mm), and an aluminum foil serving as the anode, a layer of glass fiber paper GF/D as the separator. The ionic liquid electrolyte was composed of $AlCl_3$ and [EMIm]Cl in a molar ratio of 1.3:1. The $AlCl_3$ and [EMIm]Cl were dried at 100 °C overnight to remove excess water in a nitrogen-filled glove box ($H_2O < 0.1$ppm, $O_2 <$ 0.1 ppm) before use. The cathode slurry was prepared by mixing 80 wt% active material, 10 wt% carbon black and 10 wt% polystyrene in N-methyl-2-pyrrolidone uniformly. The slurry was coated on the molybdenum collector and dried overnight at 60 °C in vacuum oven. The mass loading of active material is about 0.8~1.2 mg cm^{-2}, and the electrode thickness is approximately 150 μm. The Swage lok cells were assembled in a glove box and 150 ul of electrolyte was added to fully wet the separator. Galvanostatic charge discharge (GCD) test of the battery was performed on the LAND CT2001A battery test system at voltage ranges from 0.1 V to 2.0 V. Cyclic voltammetry (CV) was performed using an electrochemical workstation (CHI 760E).

DFT calculations

Density functional theory (DFT) calculations were conducted to optimize the configuration of atoms. The generalized gradient approximation (GGA) and the Perdew–Burke–Ernzerhof (PBE) functional was used as the exchange correlation functional. The cutoff energy was set as 450 eV, and the structure was fully relaxed until the convergence criteria of energy and force reached 1×10^{-5} eV and 0.03 eV $Å^{-1}$, respectively. In order to eliminate the interaction between the periodic structures of the surface model, a 15 Å vacuum layer was constructed. The 1 × 1 × 1 Monkhorst–Pack grid *k*-points was performed to integrate total energy in the Brillouin zone.

Figures and Tables

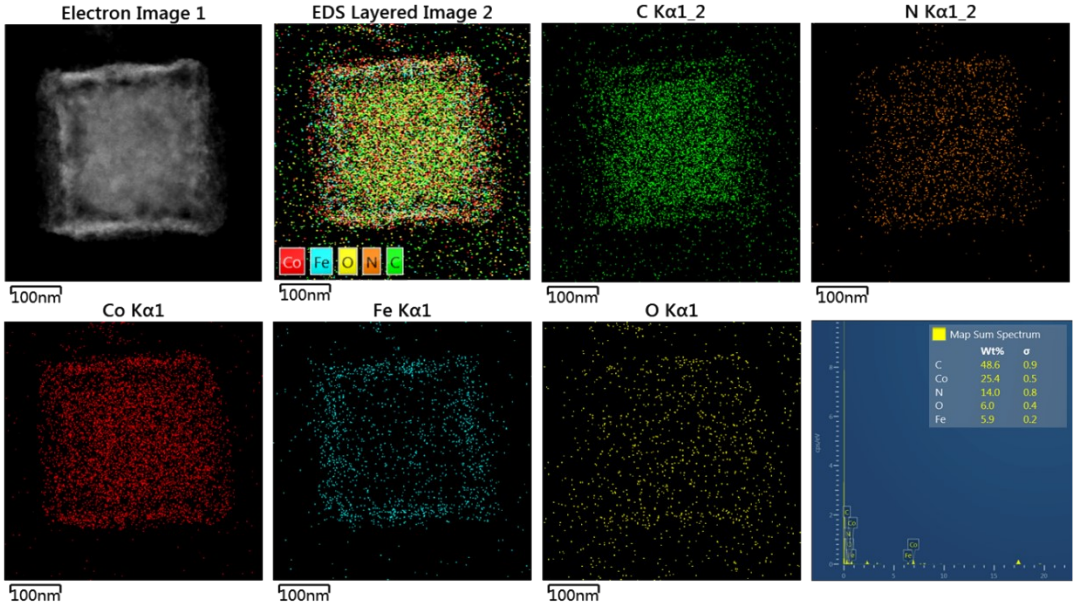

Fig. S1 The TEM image, element mapping, and EDS analysis of ZIF-67/Co-Fe PBA MOF-on-MOF precursor.

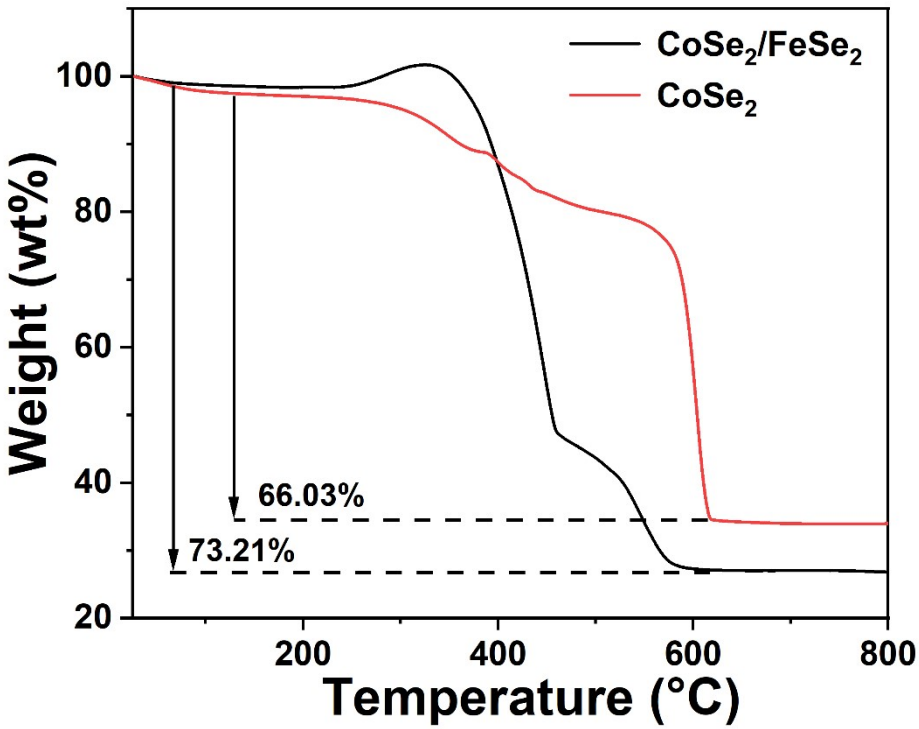

Fig. S2 The TGA curves of $CoSe_2/FeSe_2$ heterostructure and single-phase $CoSe_2$.

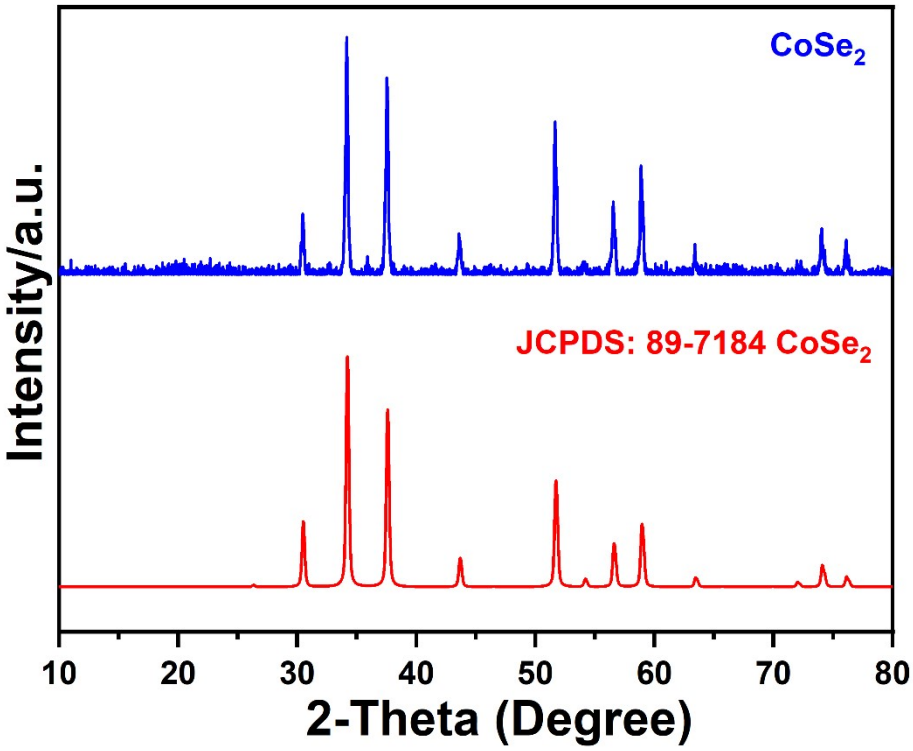

Fig. S3 The XRD pattern of the single phase $CoSe_2$.

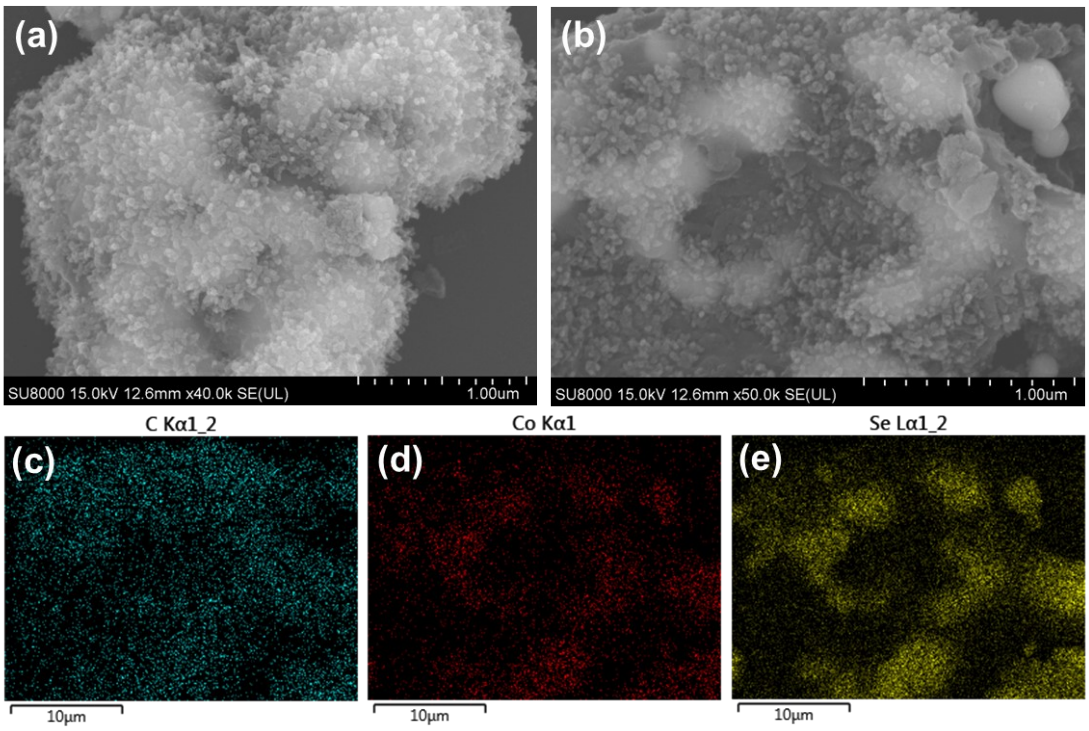

Fig. S4 The SEM images and element mapping (C, Co and Se) of the single-phase $CoSe_2$ material.

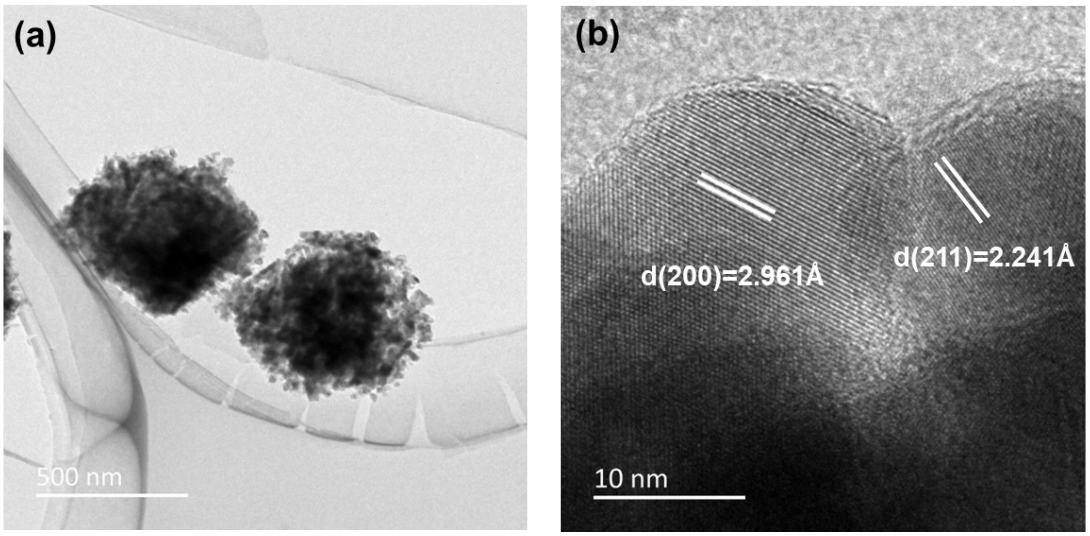

Fig. S5 The TEM image and HRTEM image of the single-phase $CoSe_2$ material.

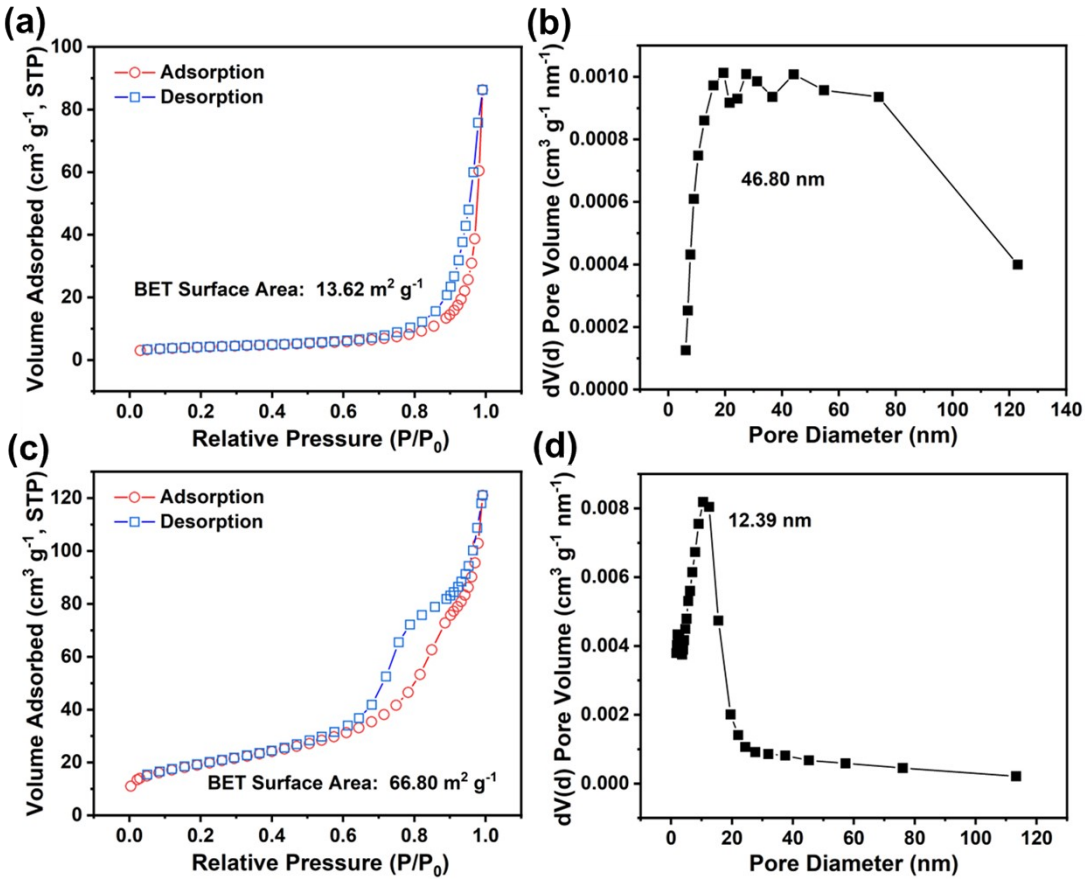

Fig. S6 The nitrogen adsorption and desorption isotherms and pore diameter distribution curves of the single-phase $CoSe_2$ (a, b) and $CoSe_2/FeSe_2$ heterostructure (c, d).

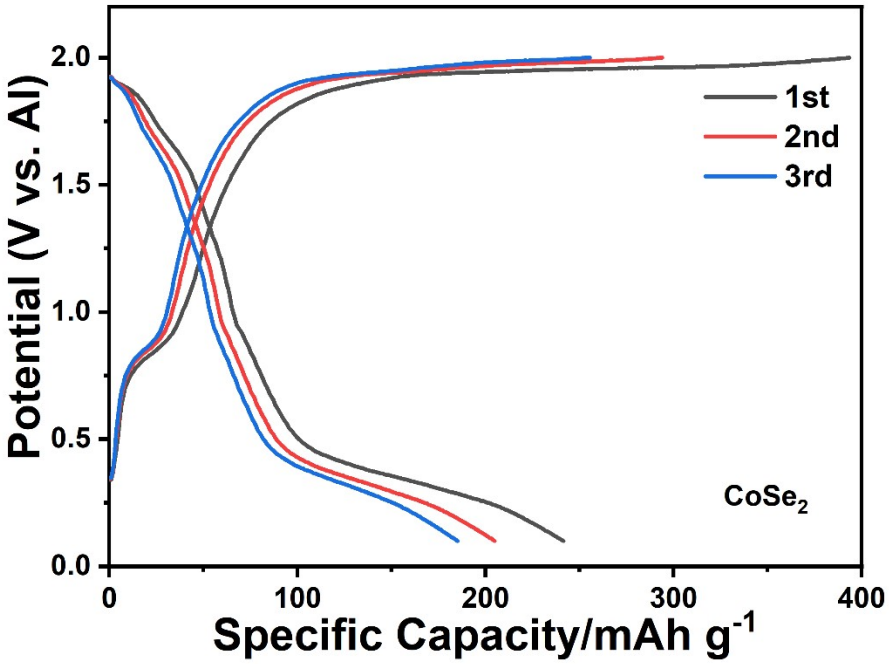

Fig. S7 The GCD curves at 100 mA g^{-1} of $CoSe_2$ in the first three cycles.

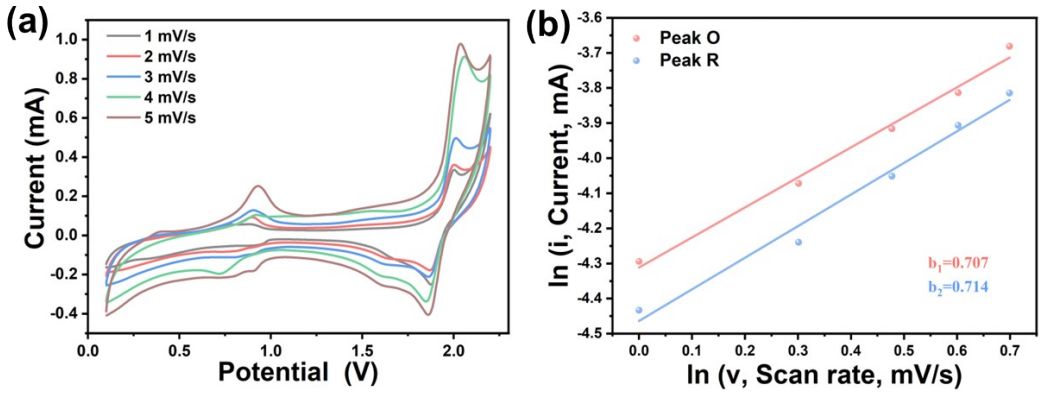

Fig. S8 The CV curves of $CoSe_2$ at the scan rate of 1-5 mV s^{-1}, and the corresponding ln (i) versus ln (v) plots.

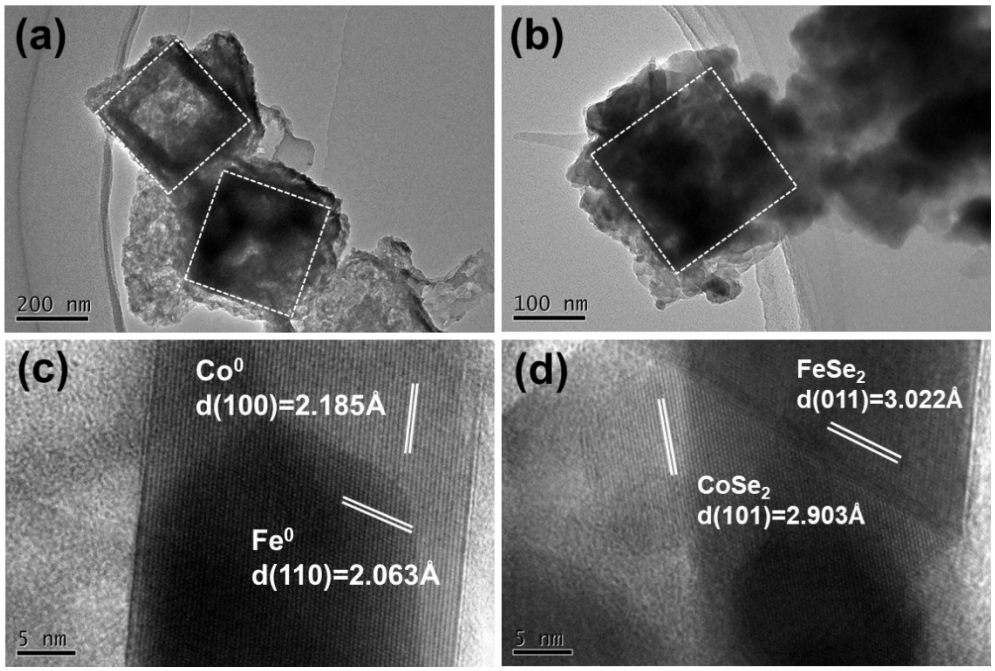

Fig. S9 Ex situ TEM images of $CoSe_2/FeSe_2$ electrode morphology after 200th cycled and HRTEM of fully discharged and charged states.

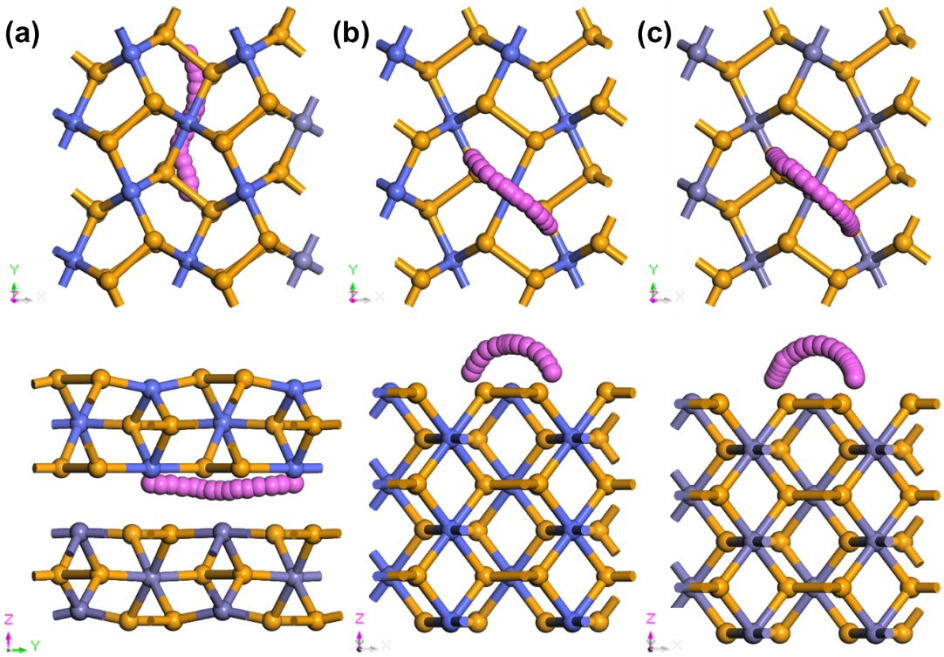

Fig. S10 The Al-ion migration path in the (a) $CoSe_2/FeSe_2$ heterostructure, (b) $CoSe_2$, and (c) $FeSe_2$ with the top view (top) and side view (bottom).

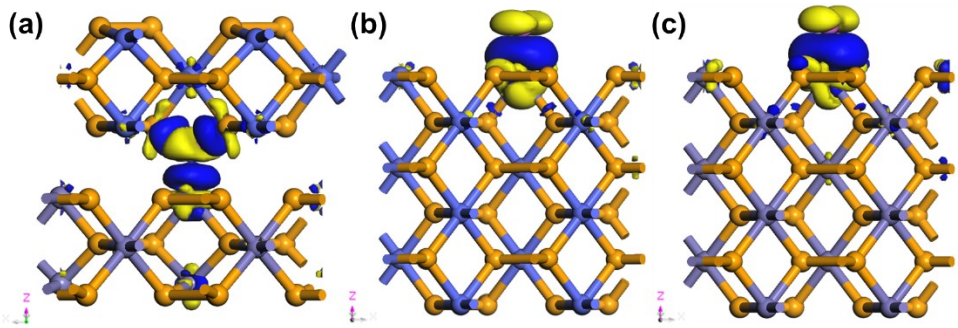

Fig. S11 The electron density difference of (a) $CoSe_2/FeSe_2$ heterostructure, (b) $CoSe_2$, and (c) $FeSe_2$ with the side view. The diagram highlights electron loss in yellow and electron enrichment in blue.

Table S1. Comparison of electrochemical properties of $CoSe_2/FeSe_2$ with other cathode materials for aluminum-ion batteries.

Voltage plateau (V)	Initial Capacity (mAh g^{-1})	Cycle number	After cycling capacity (mAh g^{-1})	Cathode material	Reference number
1.8	**243.1**	**1600**	**133.7**	**$CoSe_2/FeSe_2$**	**This work**
1.9	254.8	100	62.4	CoSe@C	[1]
2.0	326	500	143	$CoSe_2$/C-ND@rGO	[2]
1.8	582	500	145	$FeSe_2$@GO	[3]
1.2	207	500	116.8	Co_3Se_4/ZnSe	[4]
1.6	582	100	107	SnSe	[5]
0.68	287.9	150	90	Co_3S_4	[6]
0.6	180	140	116	$FeSe_2/MoS_2$	[7]
1.2	317.2	100	141.3	$Fe_{0.4}Co_{0.6}S$/NC	[8]
1.1	257.9	400	85.1	Co-P/CC	[9]
1.7	386.7	150	124	$ZnSe/SnSe_2$	[10]

Reference

1. W. Xing, D. Du, T. Cai, X. Li, J. Zhou, Y. Chai, Q. Xue and Z. Yan, *Journal of Power Sources*, 2018, **401**, 6-12.
2. T. Cai, L. Zhao, H. Hu, T. Li, X. Li, S. Guo, Y. Li, Q. Xue, W. Xing, Z. Yan and L. Wang, *Energy & Environmental Science*, 2018, **11**, 2341-2347.
3. H. Wang, L. Zhao, H. Zhang, Y. Liu, L. Yang, F. Li, W. Liu, X. Dong, X. Li, Z. Li, X. Qi, L. Wu, Y. Xu, Y. Wang, K. Wang, H. Yang, Q. Li, S. Yan, X. Zhang, F. Li and H. Li, *Energy & Environmental Science*, 2022, **15**, 311-319.
4. T. Liu, G. Lv, M. Liu, C. Zhao, L. Liao, H. Liu, J. Shi, J. Zhang and J. Guo, *ACS Applied Materials & Interfaces*, 2023, **15**, 11906-11913.
5. Y. Zhang, B. Zhang, J. Li, J. Liu, X. Huo and F. Kang, *Chemical Engineering Journal*, 2021, **403**.
6. H. Li, H. Yang, Z. Sun, Y. Shi, H.-M. Cheng and F. Li, *Nano Energy*, 2019, **56**, 100-108.
7. B. Zhang, R. Kang, W. Zhou, Y. Du, H. Wang, J. Wan and J. Zhang, *ACS Applied Energy Materials*, 2023, **6**, 3366-3373.
8. J. Zheng, S. Ju, G. Xia, H. Pan and X. Yu, *ACS Applied Materials & Interfaces*, 2022, **14**, 8076-8085.
9. S. Lu, M. Wang, F. Guo, J. Tu, A. Lv, Y. Chen and S. Jiao, *Chemical Engineering Journal*, 2020, **389**.
10. J. Li, W. Luo, Z. Zhang, F. Li, Z. Chao and J. Fan, *Journal of Colloid and Interface Science*, 2023, **639**, 124-132.